# Random sequential adsorption of coupled three-circle objects for various radius ratios

Pradip B. Shelke[1] and A. V. Limaye[2]
[1]*Department of Physics, Ahmednagar College, Ahmednagar 414 001, India*
[2]*Center for Advanced Studies in Materials Science and Solid State Physics, Department of Physics, University of Pune, Pune 411 007, India*

(Received 20 January 2011; revised manuscript received 26 April 2011; published 30 June 2011)

We study random sequential adsorption (RSA) of coupled three-circle objects (consisting of two circular discs of radius $r_2$ touching the central one of radius $r_1$ making an angle $\theta$) on a two-dimensional continuum substrate. For all the objects corresponding to various values of radius ratios $r_2/r_1$ and angles $\theta$, approach of instantaneous coverage $\Theta(t)$ to the jammed state coverage $\Theta(\infty)$, is found to obey a power law $\Theta(\infty) - \Theta(t) \sim t^{-p}$, as expected based on general arguments. However, the observed values of exponent $p$ and jammed state coverage $\Theta(\infty)$ are found to vary with $r_2/r_1$ and $\theta$. The interplay between the degree of nonconvexity $|\delta|$ and packing efficiency $\eta$ of the object governs the saturation coverage $\Theta(\infty)$.

DOI: 10.1103/PhysRevE.83.061607 PACS number(s): 68.43.Mn, 68.43.De, 82.20.Wt

## I. INTRODUCTION

The random sequential adsorption (RSA) model [1] is one of the most studied models in the context of irreversible adsorption of macromolecules on a solid substrate. The RSA model has been applied to explain adsorption of a variety of entities ranging from simple gas molecules, latex spheres, and colloidal particles to complex entities such as polymer chains, bacteria, proteins, and DNA in physics, chemistry, and biology [2]. Recently the model has been applied to a wide horizon of problems such as data processing [3], adsorption-induced diffusion, aggregation, unfolding of proteins [4], and particle branching in impact ionization [5].

The RSA model considers random and sequential addition of particles on a $d$-dimensional substrate such that at each time step only one attempt of a single particle is tried for adsorption. The attempt of adsorption is either discarded if the newly adding particle overlaps with any of the already adsorbed ones, or else the particle is rigidly fixed to the substrate. In this model as the process of addition of particles proceeds with time, the instantaneous surface coverage $\Theta(t)$ increases, and the adsorption probability decreases due to exclusion effects from preadsorbed objects until, eventually, it is impossible to place any more objects without overlap. This condition, associated with a zero probability of adsorption, is known as the jamming limit, and the coverage in the jammed state is called the jammed state coverage $\Theta(\infty)$. The approach of instantaneous coverage $\Theta(t)$ to this jammed state coverage $\Theta(\infty)$ is a matter of considerable interest for science and technology. It has been established that a power-law approach of $\Theta(t)$ to $\Theta(\infty)$, namely, $\Theta(\infty) - \Theta(t) \sim t^{-p}$ in a late time regime, is a universal behavior [6]. However, the value of exponent $p$ is found to be object shape dependent [7–10]. The RSA of objects with different shapes has been studied previously with an emphasis on obtaining the exponent $p$ value that governs the RSA dynamics. By studying RSA of objects of different shapes such as circular, elliptical, rectangular, and sphero-cylindrical, researchers have put forward some laws regarding the value of exponent $p$ [8–10]. Feder [8] was the first to relate the observed value of exponent $p$ in the case of RSA of two-dimensional circular discs to the object dimensionality and to suggest the general law $p = 1/d$ for $d$-dimensional spheres on a $d$-dimensional continuum substrate. Swendsen [9] further showed that the same should also hold for RSA of objects of any arbitrary shape provided that the objects are dropped with random orientations. However, P. Viot and G. Tarjus [10] in their simulation results for RSA of unoriented squares found that Swendsen's conjecture $p = 1/d$ is not valid and stated the relation $p \sim 1/d_f$, $d_f$ being the degrees of freedom of the adsorbing object.

In so far as the object shape is concerned the finite area objects can be categorized in two classes, viz., convex-shaped objects and nonconvex-shaped objects. Geometrically convex shaped objects are singly connected objects in the sense that the line segment joining any two interior points lies wholly in the interior of the object, while nonconvex-shaped objects are not singly connected. We pointed out in our recent work [11] that the above mentioned laws regarding the value of exponent $p$ were arrived at by carrying out RSA of convex shape objects only. We therefore examined RSA of nonconvex objects for the first time to check the validity of the law $p \sim 1/d_f$ using nonconvex coupled three- and two-circle objects [11]. By carrying out computer simulations for these objects on two-dimensional continuum substrate we showed that the argument $p \sim 1/d_f$ is not valid for nonconvex objects. To quantify the degree of nonconvexity, we defined a quantity, termed as the coefficient of departure from convexity $\delta$ and showed that the departure from the law $p \sim 1/d_f$ has a good direct correlation with this quantity. It was observed that the objects with different degree of nonconvexity have different values of exponent $p$. This variation in $p$ was also shown to get reflected in the variation of the number of adsorbed particles at any given time instant. This interesting fact was also shown to be relevant to the issue of targeted drug delivery [11].

The coupled three-circle object considered in our previous study consisted of three identical circular discs, each of radius $r$(two circles touching the central one making an angle $\theta$). The present paper is an extension of previous study wherein we study RSA of a more general type of coupled three-circle

 

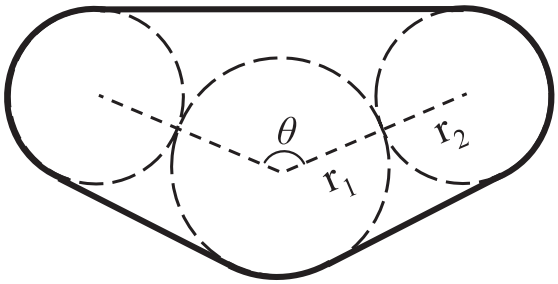


FIG. 1. Coupled three-circle object shown with dotted lines, and the solid thick curves show the convex shape of minimum area enclosing the object.

object with variation in the relative size of the central circular disc vis-à-vis the two coupling side circular discs (of the same size) (Fig. 1).

## II. MODEL

A plane continuum substrate of area $A = L \times L$ is considered. The object considered for adsorption is a coupled three-circle object of area $a$. At each time step one object with random position and orientation is tried for adsorption. The object gets successfully adsorbed if it does not overlap with previously adsorbed ones; otherwise it is rejected. In either case, time is incremented by one unit. For fixed $a/A$ ratio the simulations are carried out for different sets of radius ratio $r_2/r_1$ and angle $\theta$. The range of values of $r_2/r_1$ studied is from 0.1 to 1, and $\theta$ values studied are $\theta = 180^\circ$, $150^\circ$, $120^\circ$, $90^\circ$, and $60^\circ$. For each set of values of $\theta$ and $r_2/r_1$, simulations are carried out up to $2\times10^8$ time steps, and results are obtained by averaging over 10 simulation runs. The $a/A$ ratio is kept low enough to minimize the finite size effects ($a/A = 0.00004$). Also, periodic boundary conditions are applied to eliminate boundary effects.

## III. RESULTS AND DISCUSSION

Figure 2 shows a representative graph of coverage $\Theta(t)$ versus time $t$ for radius ratio $r_2/r_1 = 0.5$ and $\theta = 60^\circ$. The graph shows a rapid increase in coverage value in the early time regime indicating that almost all adsorption attempts succeed. This is further evident from the slope value of the linear fit being close to 1 (see inset). In the intermediate time regime there is a slowing down in the rate of increase of coverage, followed by the asymptotic regime in which the coverage reaches a constant value $\Theta(\infty)$.

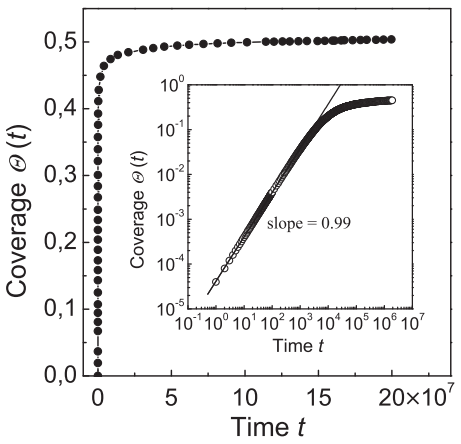


FIG. 2. Representative plot of coverage $\Theta(t)$ vs time $t$ for radius ratio $r_2/r_1 = 0.5$ and $\theta = 60^\circ$. Inset graph shows variation of coverage $\Theta(t)$ vs time $t$, on a log-log scale, in an early time regime.

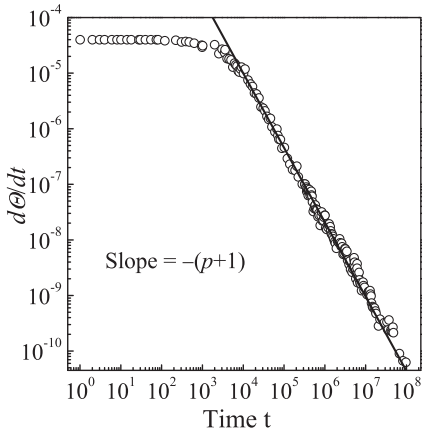


FIG. 3. Plot of $d\Theta(t)/dt$ vs time $t$ on a log-log scale.

Figure 3 shows $d\Theta(t)/dt$ versus time $t$ plot on a log-log scale. The linear nature of the graph in the asymptotic regime confirms that the kinetics of adsorption follows the law $\Theta(\infty) - \Theta(t) \sim t^{-p}$. The slope of the best-fit line to the linear part of the graph in this asymptotic regime gives the value of the exponent when equated to $-(p + 1)$.

Figure 4 shows the graph of exponent $p$ versus radius ratio $r_2/r_1$ for different values of $\theta$. In general all the graphs follow the trend that as radius ratio decreases form 1 to 0.1 (i.e., when the size of the two side discs goes on decreasing relative to the size of central one), the value of exponent $p$ approaches 0.5. This is along the expected lines, since when the radius ratio becomes zero it will be the case of adsorption of a single circular disc that has the value $p = 0.5$. Also it is to be noted that when the radius ratio is less than or equal to 0.2, values of exponent $p$ are the same (within an error limit) for different values of $\theta$, and hence approach to the jammed state is

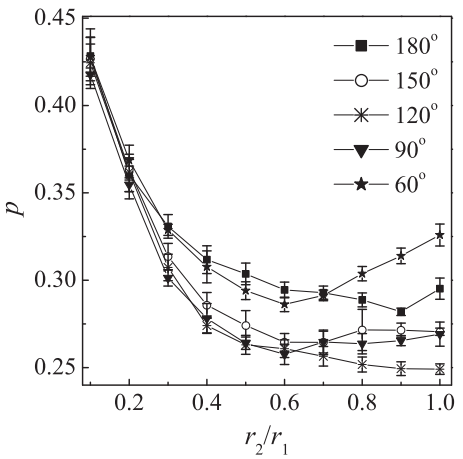


FIG. 4. Plot of exponent $p$ vs radius ratio $r_2/r_1$ for different values of $\theta$.

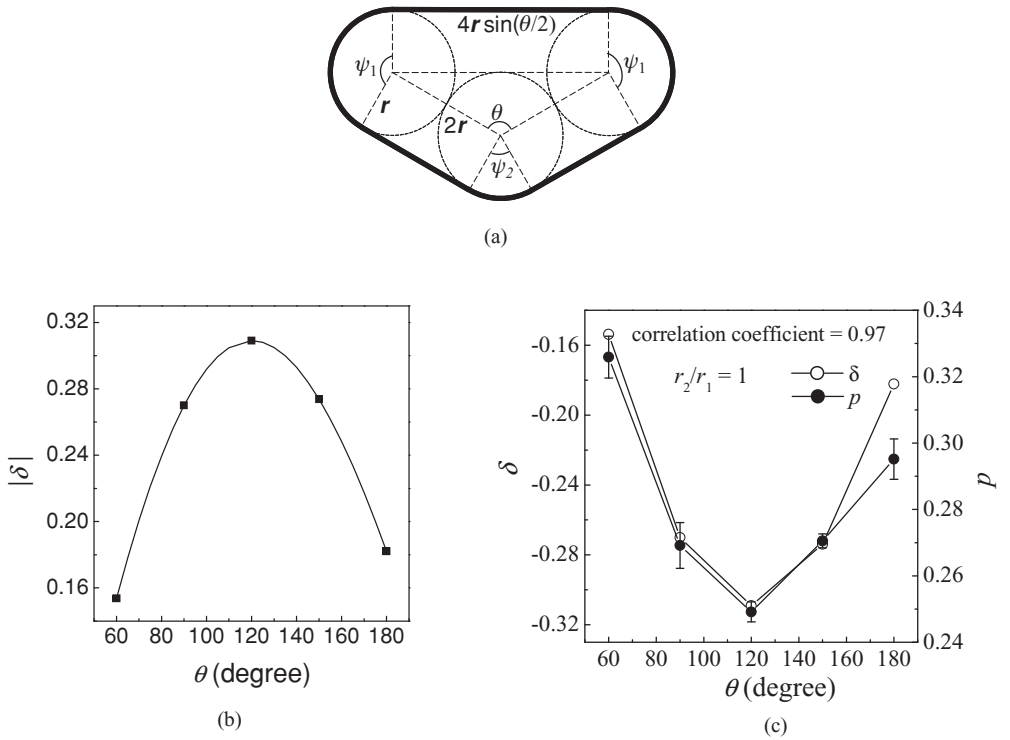


FIG. 5. (a) Convex shape circumscribing three-circle object with $r_2/r_1 = 1$. (b) Plot of absolute value of coefficient of departure from convexity $|\delta|$ vs the object angle $\theta$ for the case of $r_2/r_1 = 1$. (c) Graphs of the coefficient of departure from convexity $\delta$ and the exponent $p$ vs the object angle $\theta$ for $r_2/r_1 = 1$.

independent of angle between the discs, when the radius ratio is less than or equal to 0.2. This is because when the radius ratio is small ($\leqslant 0.2$), the radius $r_2$ of the side circular discs is too small for the angular nature to play any role. Indeed, the size of coupling discs then becomes less than the typical average gap separation in case of RSA of circular discs, and hence the role of coupling discs in affecting the kinetics of RSA becomes almost insignificant.

It is also seen from the graph that for any given value of radius ratio $r_2/r_1$, the values of the exponent $p$ for $\theta = 180^\circ$ and $60^\circ$ are higher than that for the objects corresponding to other values of $\theta$, while those for $\theta = 120^\circ$ are the least. These differences get highlighted more and more as the radius ratio approaches 1. This can be understood on the basis that the shapes of the objects corresponding to $\theta = 180^\circ$ and $60^\circ$ are closer to convex bodies, namely, rectangle and triangle, respectively, for radius ratio 1, while the shape of the object with $\theta = 120^\circ$ is far from a convex shape, an issue that is already discussed in detail in our earlier work [11].

Now let us discuss the trend of variation of $p$ with radius ratio $r_2/r_1$ for each value of angle $\theta$. The behavior of the variation of exponent $p$ in the case of an object corresponding to $\theta = 120^\circ$ is distinctly different than that for the objects corresponding to other values of $\theta$. For the objects corresponding to $\theta = 120^\circ$, there is monotonic increase in $p$ values with a decrease in the radius ratio $r_2/r_1$. On the other hand, for the objects corresponding to the other values of $\theta$, the exponent value first decreases as radius ratio decreases to a certain value and then increases with further decrease in the radius ratio. For the objects corresponding to $\theta = 60^\circ$ and $90^\circ$, the values of $p$ bottom out at $r_2/r_1 = 0.6$ and start rising as $r_2/r_1$ decreases further. In the case of the object corresponding to $\theta = 150^\circ$ the bottom is at $r_2/r_1 = 0.7$, whereas in the case of the object corresponding to $\theta = 180^\circ$, it bottoms out when $r_2/r_1 = 0.9$.

Let us now consider the case of objects with $\theta = 60^\circ$ and $90^\circ$. Out of these two objects, the object with $\theta = 60^\circ$ has a lesser degree of nonconvexity than that for other objects ($\theta = 90^\circ, 120^\circ, 150^\circ$ and $180^\circ$). For radius ratio 1, the object is more convex, and it has a $p$ value close to 0.33, i.e., $1/d_f$. But as the radius ratio decreases, its degree of nonconvexity increases, and so there is a fall in $p$ values up to $r_2/r_1 = 0.6$. The behavior of $p$ in this regime of radius ratio can be better explained as follows: The object with $\theta = 60^\circ$ and $r_2/r_1 = 1$ is closed, and its crevices resemble the crevices in the case of a coupled two-circle object [11]. In the case of coupled two-circle objects there is crossover between the area of crevice and the area of smaller circle at radius ratio 0.6 [for reference see inset of Fig. 4(b) in Ref. [11]) The same effect is applicable in the case of a coupled three-circle object with $\theta = 60^\circ$. On the other hand, for $r_2/r_1 \leqslant 0.3$, the size of two smaller side circles becomes more and more insignificant, and the $p$ value starts rising rapidly, with the decrease in $r_2/r_1$, in order to reach the value of 0.5, which happens to be the $p$ value for RSA of circular discs (when $r_2/r_1 = 0$).

The same reasoning is applicable for the variation of exponent values of the objects corresponding to $\theta = 90^\circ$. However, in this case it has more of a degree of nonconvexity as compared with the object corresponding to $\theta = 60^\circ$, so its $p$ values are less than that for the object with $\theta = 60^\circ$.

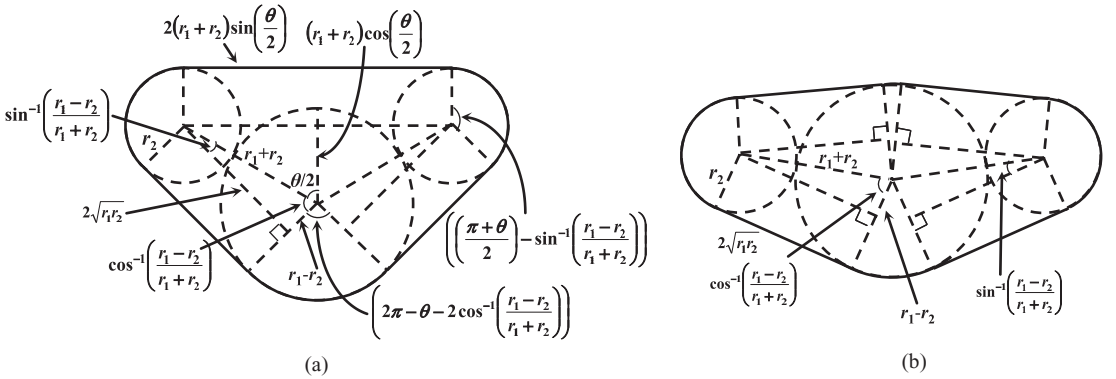


FIG. 6. Convex shape circumscribing three-circle object: Case (a) $\theta \leqslant 2\cos^{-1}(\frac{r_1-r_2}{r_1+r_2})$ and Case (b) $\theta \geqslant 2\cos^{-1}(\frac{r_1-r_2}{r_1+r_2})$.

In the case of object with $\theta = 150^\circ$ and $180^\circ$ the minimum in the $p$ value occurs at radius ratio 0.7 and 0.9, respectively, the values being somewhat higher than that in case of the objects with $\theta = 60^\circ$ and $90^\circ$, for which the minimum is at 0.6. This may be because these objects are more open in the sense that in the case of these objects, the attached circles are wide apart from each other compared with that for other values of $\theta$. Also the object with $\theta = 180^\circ$ has less degree of nonconvexity, which would explain why $p$ values for $\theta = 180^\circ$ are higher than that for $\theta = 150^\circ$, as mentioned earlier.

The above discussion of the simulation results and analysis, which basically involves the qualitative arguments, clearly highlights that most of the behaviors can be understood on the basis of the degree of nonconvexity of the object. To strengthen the point, we now present the quantitative analysis. For this purpose we quantify the degree of nonconvexity by defining the "coefficient of departure from convexity," $\delta$. We consider the closest convex shape of minimum area that circumscribes the coupled three-circle object, as shown in Fig. 5(a). We then define $\delta$ as the difference in the area of a coupled three-circle object and the area of the circumscribing convex shape per unit area of the coupled three-circle object [11].

When $r_2/r_1 = 1$ [Fig. 5(a)],

$$\delta(r_2/r_1,\theta) = \left\{a - \left[4r^2 + 4r^2\sin(\theta/2) + 4r^2\sin(\theta/2)\cos(\theta/2) + r^2\psi_1 + \frac{1}{2}r^2\psi_2\right]\right\}\Big/ a,$$

where $\psi_1 = (\pi + \theta)/2$ and $\psi_2 = \pi - \theta$ and $a$ is the area of the object, with $\theta$ expressed in radians. $\delta(r_2/r_1,\theta)$ is minimum (or equivalently, the absolute value of coefficient of departure from convexity $|\delta|$ is maximum) when $\theta = 120^\circ$. Thus, the object with $\theta = 120^\circ$ has the highest degree of nonconvexity, i.e., this object is the one that is farthest away from the convex shape and hence has the lowest value of the exponent $p$. Figure 5(b) shows the plot of the absolute value of the coefficient of departure from convexity $|\delta|$ versus the object angle $\theta$, and Fig. 5(c) shows the graphs of the coefficient of departure from convexity $\delta$ and the exponent $p$ versus the object angle $\theta$, for $r_2/r_1 = 1$. An excellent overlap, especially for $\theta$ values less or equal to $150^\circ$, implies a good correlation between the plotted quantities. In fact, the correlation coefficient is found to be 0.97, which can be termed the near perfect positive correlation between $\delta$ and $p$.

When $r_2/r_1 \neq 1$, for object area $a$, two different cases arise as shown in Fig. 6:

Case (a). When $\theta \leqslant 2\cos^{-1}(\frac{r_1-r_2}{r_1+r_2})$, we have $\delta(r_2/r_1,\theta) = [a - (A + B + C + D + E)]/a$, where $A = 2\sqrt{r_1r_2}(r_1 + r_2)$, $B = 2r_2(r_1+r_2)\sin(\frac{\theta}{2})$, $C = \frac{1}{2}(r_1+r_2)^2\sin\theta$, $D = r_2^2[(\frac{\pi+\theta}{2}) - \sin^{-1}(\frac{r_1-r_2}{r_1+r_2})]$, and $E = \frac{1}{2}r_1^2[(2\pi - \theta) - 2\cos^{-1}(\frac{r_1-r_2}{r_1+r_2})]$, $\theta$ being expressed in radians.

Case (b). When $\theta \geqslant 2\cos^{-1}(\frac{r_1-r_2}{r_1+r_2})$, we have $\delta(r_2/r_1,\theta) = [a - (F + G + H)]/a$, where $F = 4\sqrt{r_1r_2}(r_1 + r_2)$, $G = \frac{1}{2}r_2^2[2\pi - 4\sin^{-1}(\frac{r_1-r_2}{r_1+r_2})]$, and $H = \frac{1}{2}r_1^2[2\pi - 4\cos^{-1}(\frac{r_1-r_2}{r_1+r_2})]$, $\theta$ being expressed in radians.

For a given value of $r_2/r_1$, the minimum value of $\delta(r_2/r_1,\theta)$ occurs when $\theta = 2\cos^{-1}(\frac{1}{1+r_2/r_1})$. Figure 7 shows the plots of the absolute value of the coefficient of departure from convexity $|\delta|$ versus the object angle $\theta$ for three representative values of $r_2/r_1$, namely, $r_2/r_1 = 0.7$, 0.4, and 0.1, while Figure 8 shows the graphs of the coefficient of departure from convexity $\delta$ and the exponent $p$ versus the object angle $\theta$, for

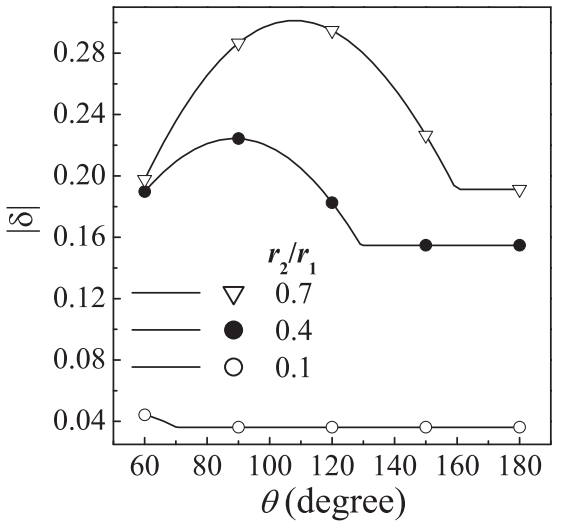


FIG. 7. Plots of absolute value of coefficient of departure from convexity $|\delta|$ vs the object angle $\theta$ for three representative values: $r_2/r_1 = 0.7$, 0.4, and 0.1.

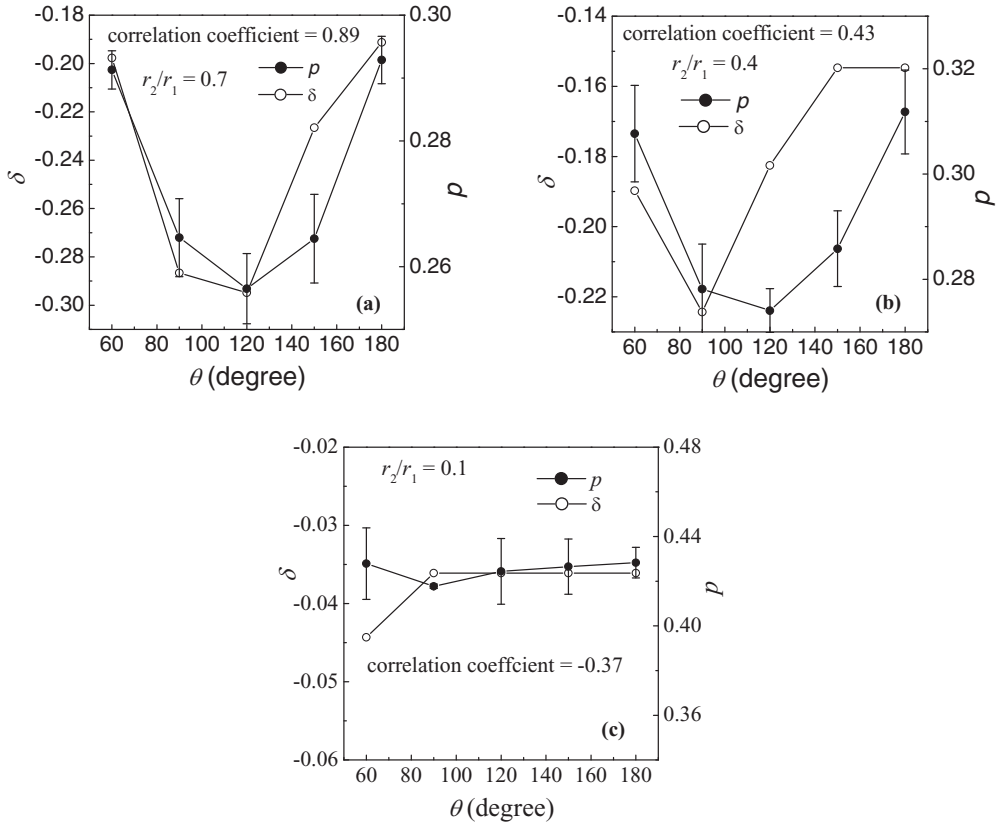


FIG. 8. Graphs of the coefficient of departure from convexity $\delta$ and the exponent $p$ vs the object angle $\theta$, for $r_2/r_1 = 0.7$ (a), 0.4 (b), and 0.1 (c).

these three representative values of $r_2/r_1$. It is clearly seen that for the case of $r_2/r_1 = 0.7$, $\delta$ and $p$ follow the identical trends and have good correlation with the coefficient value of 0.89. For the case of $r_2/r_1 = 0.4$, the correlation coefficient is 0.43, signifying weak positive correlation between $\delta$ and $p$. For the case of $r_2/r_1 = 0.1$, the correlation is negative and weak but does not signify much as both $\delta$ and $p$ do not show any significant dependence on the object angle $\theta$ due to the fact that size of the side circles is so small that they do not play any significant role. In fact, what we have observed is that the correlation goes on weakening with the decrease in the radius ratio from 1 to 0.1 (see Table I).

Figure 9 shows the graphs of the coefficient of departure from convexity $\delta$ and the exponent $p$ versus the radius ratio $r_2/r_1$ for three representative values of object angle $\theta$; $\theta = 60^\circ$, $120^\circ$, and $180^\circ$, respectively. It is quite clear from these graphs that in each of these cases the trends followed by $\delta$ and $p$ are identical. This gets further established from the fact that for $\theta = 60^\circ$, $120^\circ$, and $180^\circ$, the correlation coefficients are found to be 0.99, 0.93, and 0.98, respectively, indicating near perfect positive correlation between $\delta$ and $p$. We have also determined the correlation coefficients for the cases $\theta = 90^\circ$ and $150^\circ$, which are found to be 0.97 and 0.88, respectively.

TABLE I. Values of correlation coefficients for different values of $r_2/r_1$.

| $r_2/r_1$ | Correlation coefficient |
|---|---|
| 1 | 0.97 |
| 0.9 | 0.92 |
| 0.8 | 0.97 |
| 0.7 | 0.89 |
| 0.6 | 0.73 |
| 0.5 | 0.71 |
| 0.4 | 0.43 |
| 0.3 | 0.20 |
| 0.2 | −0.45 |
| 0.1 | −0.37 |

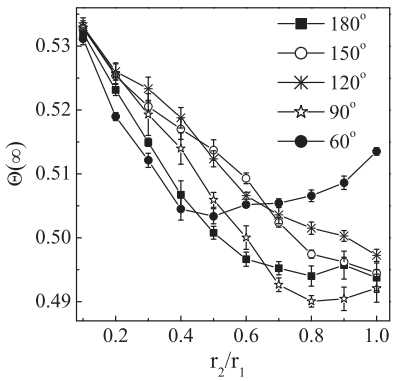


FIG. 10. Jammed state coverage $\Theta(\infty)$ vs radius ratio $r_2/r_1$ for different values of $\theta$.

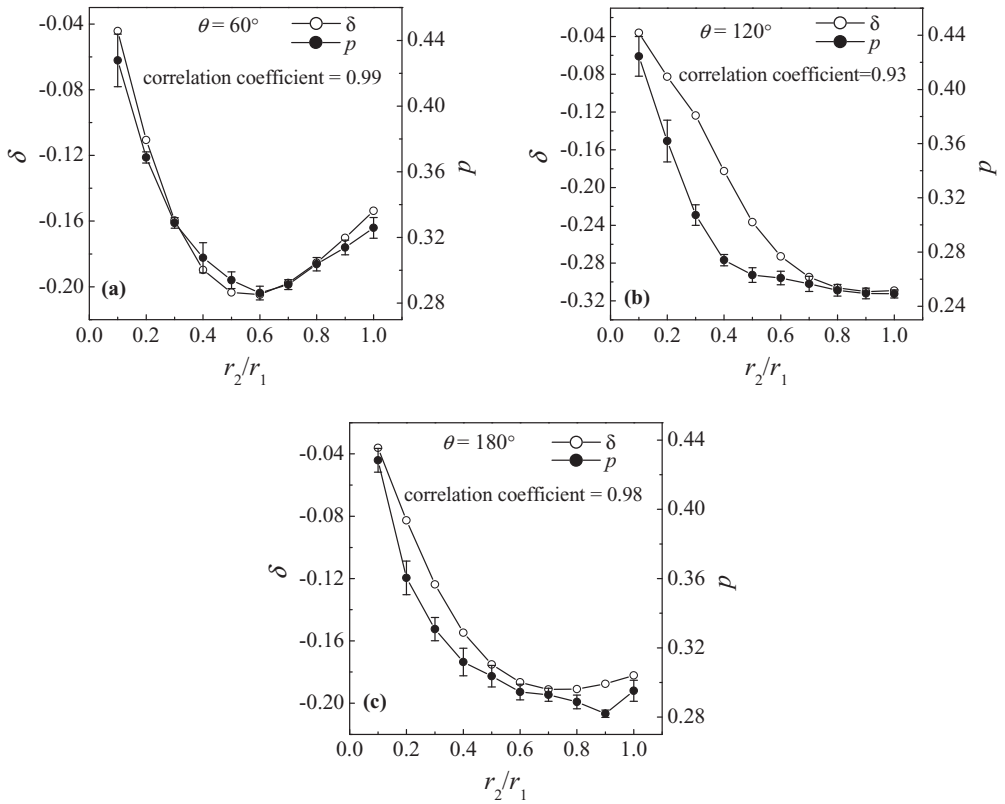


FIG. 9. Graphs of the coefficient of departure from convexity $\delta$ and the exponent $p$ vs the radius ratio $r_2/r_1$ for three representative values of object angle $\theta$: $\theta = 60^\circ$ (a), $120^\circ$ (b), and $180^\circ$ (c).

The above discussed quantitative analysis hence clearly highlights the significant role of the coefficient of departure from convexity $\delta$ in governing the late time regime dynamics of RSA of nonconvex-shaped objects.

Jammed state coverage $\Theta(\infty)$ is yet another quantity that is of significance and has been studied extensively by many researchers. Figure 10 shows variation of jammed state coverage $\Theta(\infty)$ versus radius ratio $r_2/r_1$ for different values of $\theta$. Before understanding how radius ratio $r_2/r_1$ influences the jammed state coverage $\Theta(\infty)$, we will first discuss the $\theta$ dependence of the jammed state coverage $\Theta(\infty)$.

For this purpose, consider the case of radius ratio $r_2/r_1 = 1$. Figure 11 shows the plot of $\Theta(\infty)$ as a function of $\theta$

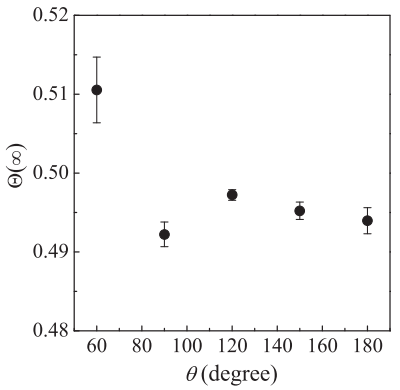


FIG. 11. Plot of jammed state coverage $\Theta(\infty)$ vs the object angle $\theta$ for radius ratio $r_2/r_1 = 1$.

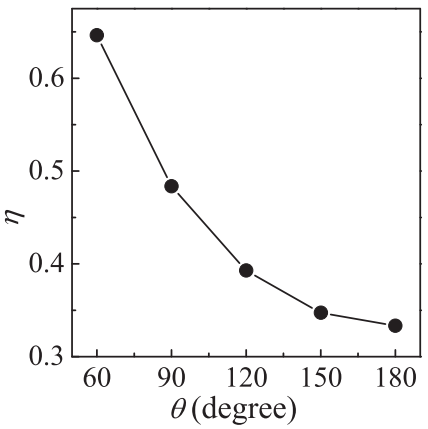


FIG. 12. Plot of packing efficiency factor $\eta$ vs the object angle $\theta$ for the case of $r_2/r_1 = 1$.

for this case of $r_2/r_1 = 1$. As seen in the figure, $\Theta(\infty)$ goes on increasing for $\theta$ decreasing from $180^\circ$ to $120^\circ$, then drops to minimum for $\theta = 90^\circ$, and again increases, becoming maximum when $\theta$ becomes $60^\circ$. This behavior can be understood as follows: In the case of elongated objects, there is more wastage of the substrate space due to random orientations of the adsorbed objects as compared with that for compact objects. This results in a lower value of saturation coverage for elongated objects. This influence is measured by the packing efficiency factor, $\eta$, given by the ratio of the actual area covered by the object to the area swept by the object in complete rotation [12]. The plot of packing efficiency factor

$\eta$ versus $\theta$, for the case of radius ratio $r_2/r_1 = 1$, is shown in Fig. 12. There is clear monotonic increase in $\eta$ as $\theta$ goes on decreasing from 180° to 60°, and hence if packing efficiency factor $\eta$ alone would have been the factor influencing the jammed state coverage $\Theta(\infty)$, then these two quantities would have shown same trends. However, Figs. 11 and 12 clearly show that this is not the case. This is due to the nonconvex nature of the objects, which is measured by $|\delta|$. It seems that in case of nonconvex objects there is an interplay between $\eta$ and $|\delta|$ that governs $\Theta(\infty)$. If the absolute value of the coefficient of the departure from convexity, $|\delta|$, is high, then as discussed earlier the newly coming object can get adsorbed with closer proximity when compared with the case of convex object [11]. Thus, the jammed state coverage is expected to be better in the case of objects with larger value of $|\delta|$. However, it is clearly not that simple, because, in the case of convex objects, that area of the convex object, which is outside the nonconvex object, gets measured, but not in case of nonconvex object, while arriving at the value of $\Theta(\infty)$. Hence there is some wastage of space in case of RSA of a nonconvex object. If the nonconvex object getting adsorbed in the vicinity can go much closer to the adsorbed object, then this wastage would be less, and would be more otherwise. Of course, all this depends on the object shape. In the case of a coupled three-circle object with radius ratio $r_2/r_1 = 1$, for $\theta = 60°$ and 180°, this type of wastage is minimal and is maximum for $\theta = 90°$, whereas for $\theta = 120°$ and 150°, the two side circles create a wide opening between them, allowing more proximity to the newly arriving object, when compared with $\theta = 90°$. Hence, for these $\theta$ values, this type of wastage is moderate, i.e., lower than that for $\theta = 90°$ and more than that for $\theta = 60°$ and 180°.

Coming to $r_2/r_1$ dependence of the saturation coverage, it is clearly noticed in Fig. 10 that except for the case of $\theta = 60°$, in all other cases the trend is similar. In each of these cases, $\Theta(\infty)$ has a low value at $r_2/r_1 = 1$, and it goes on gradually increasing with decrease in $r_2/r_1$. This trend is very much expected since with decrease in $r_2/r_1$, the side circles become smaller and smaller, thereby losing their significance. In the case of an object with $\theta = 60°$, when $r_2/r_1 = 1$, the two side circles touch each other, and wastage of space is minimal, which results in a relatively higher value of $\Theta(\infty)$ compared with that in the case of other values of $\theta$. However, as $r_2/r_1$ becomes less than 1, the two side circles do not touch each other, and hence wastage starts increasing with a decrease in $r_2/r_1$. Due to this reason, $\Theta(\infty)$ goes on decreasing till $r_2/r_1 = 0.5$. Below this value with $r_2/r_1$ approaching zero the role of side circles becomes more and more insignificant, and $\Theta(\infty)$ tends to the value of that in the case of circular discs.

Last, we wish to add a comment: Tarjus *et al.* [13] have shown that the configurations generated by the equilibrium filling process (in which the adsorbed particles diffuse and the system relaxes to equilibrium between the successive additions) and RSA (in which the adsorbed particles get rigidly fixed) differ in many respects. In the context of rate of adsorption $d\Theta(t)/dt$ being expressed as a series in increasing powers of instantaneous coverage $\Theta(t)$, Widom [14] demonstrated that the two processes are indistinguishable up to second order in $\Theta(t)$, making the coefficient of $\Theta^3(t)$ to be most significant when it comes to differentiate between the two processes. Schaff and Talbot derived exact analytic expressions for the first three coefficients and have shown that at least for the two-dimensional case, a virial-like expansion up to third order describes the low- and intermediate-regime kinetics of RSA with high accuracy [15,16]. They further extended the work to higher dimensions also [16].

In the light of the importance of these works, it will be interesting to carry out similar studies for RSA of nonconvex objects. However, the present work has its focus on an asymptotic regime and not on early and intermediate regimes, and hence we plan to carry out these investigations as a separate work, and if we are successful, our results will be presented as a future communication.

## IV. CONCLUSION

In conclusion, in the case of nonconvex objects like the coupled three-circle object, the approach to a jammed state is found to follow a power law $\Theta(\infty) - \Theta(t) \sim t^{-p}$ for various values of the radius ratio. We find that the observed values of exponent $p$ and $\Theta(\infty)$ for various values of the radius ratio $r_2/r_1$ and the angle $\theta$ show characteristic variation. The interplay between the quantities' packing efficiency factor and the ability of the object to allow the other object to get adsorbed in its proximity without overlapping it (i.e., the coefficient of departure from convexity $\delta$) governs the value of $\Theta(\infty)$.

## ACKNOWLEDGMENTS

PBS acknowledges UGC (India), and AVL acknowledges University of Pune (India) for research grants. PBS acknowledges CDAC India for providing the computational facility.

[1] J. W. Evans, Rev. Mod. Phys. **65**, 1281 (1993); J. -S. Wang and R. B. Pandey, Phys. Rev. Lett. **77**, 1773 (1996); S. M. Ricci, J. Talbot, G. Tarjus, and P. Viot, J. Chem. Phys. **97**, 5219 (1992); J. Talbot, G. Tarjus, P. R. V. Tassel, and P. Viot, Colloids Surf. A **165**, 287 (2000); V. Privman, J. -S. Wang, and P. Nielaba, Phys. Rev. B **43**, 3366 (1991).

[2] J. J. Ramsden, Phys. Rev. Lett. **71**, 295 (1993); B. Senger *et al.*, J. Chem. Phys. **97**, 3813 (1992); P. J. Flory, J. Am. Chem. Soc. **61**, 1518 (1939); G. Y. Onoda and E. G. Linigier, Phys. Rev. A **33**, 715 (1986); J. Feder and I. Giaver, J. Colloid Interface Sci. **78**, 144 (1980).

[3] E. G. Coffman Jr., L. Flatto, P. Jelenkovich, and B. Poonen, Algorithmica **22**, 448 (1998).

[4] D. Pellenc, O. Gallet, and H. Berry, Phys. Rev. E **72**, 051904 (2005).

[5] M. Inoue, Phys. Rev. B **25**, 3856 (1982).

[6] P. B. Shelke, M. D. Khandkar, A. G. Banpurkar, S. B. Ogale, and A. V. Limaye, Phys. Rev. E **75**, 060601(R) (2007).

[7] J. Talbot, G. Tarjus, and P. Schaaf, Phys. Rev. A **40**, 4808 (1989).
[8] J. Feder, J. Theor. Biol. **87**, 237 (1980).
[9] R. Swendsen, Phys. Rev. A **24**, 504 (1981).
[10] P. Viot and G. Tarjus, Europhys. Lett. **13**, 295 (1990).
[11] P. B. Shelke, S. B. Ogale, M. D. Khandkar, and A. V. Limaye, Phys. Rev. E **77**, 066111 (2008).
[12] R. D. Vigil and R. M. Ziff, J. Chem. Phys. **91**, 2599 (1989).
[13] G. Tarjus, P. Schaaf, and J. Talbot, J. Stat. Phys. **63**, 167 (1991).
[14] B. Widom, J. Chem Phys. **44**, 3888 (1966).
[15] P. Schaaf and J. Talbot, Phys. Rev. Lett. **62**, 175 (1989); J. Chem Phys. **91**, 4401 (1989).
[16] J. Talbot, P. Schaaf, and G. Tarjus, Mol. Phys. **72**, 1397 (1991).